Journal of Applied Physics ARTICLE scitation.org/journal/jap

Influence of phonon-assisted tunneling on photovoltaic properties of $BaSi_2$ and $BaGe_2$ *p–n* homojunction solar cell devices

Cite as: J. Appl. Phys. **131**, 185001 (2022); doi: 10.1063/5.0072523
Submitted: 23 September 2021 · Accepted: 11 April 2022 ·
Published Online: 9 May 2022

Ramesh Mamindla[1,2,a)] and Manish K. Niranjan[1,b)]

AFFILIATIONS

[1]Department of Physics, Indian Institute of Technology, Hyderabad, Telangana 502285, India
[2]Department of Physics, VNR Vignana Jyothi Institute of Engineering and Technology, TS, Hyderabad 500090, India

[a)]**Author to whom correspondence should be addressed:** ramesh.mamindla@gmail.com
[b)]manish@iith.ac.in

ABSTRACT

The solar cell properties of crystalline $BaSi_2$ and $BaGe_2$ *p–n* homojunctions are explored using density functional theory combined with a nonequilibrium Green function method. In particular, the quantitative estimates of solar cell parameters such as photocurrent, open-circuit voltage (V_{oc}), short-circuit current ($|J_{sc}|$), and efficiency (η) are obtained for LDA and GGA-1/2 functionals. The effect of temperature on solar cell parameters is included through electron–phonon coupling (EPC) using the special thermal displacements method. The magnitudes of J_{sc}, V_{oc}, and η for $BaSi_2$ ($BaGe_2$) at 300 K are found to be 27.35 mA/cm^2 (26.1 mA/cm^2), 0.84 V (0.78 V), and 18.0% (16.6%), respectively. Our study strongly suggests that the phonon-assisted photon absorption and thereby EPC significantly affect the photocurrent, and its inclusion is necessary for a proper description of various solar cell parameters. The computed solar cell parameters for $BaSi_2$ ($BaGe_2$) *p–n* homojunctions can be used as benchmark *ab-initio* quantum mechanical results and can be used in simulations based on continuum models.

I. INTRODUCTION

Semiconducting silicides are an important class of materials with wide ranging technological applications.[1–5] These systems also exhibit a variety of interesting physical properties that make them quite attractive for scientific investigations as well.[1] In particular, semiconducting silicide $BaSi_2$ has generated a great deal of attention in recent years, owing to its promising applications in thermoelectric, photovoltaic, and optoelectronic devices.[6–14] $BaSi_2$ has good thermoelectric properties with high Seebeck coefficient and low thermal conductivity that are comparable to those of a conventional thermoelectric material such as Bi_2Te_3. $BaSi_2$ has also emerged as a promising photovoltaic material due to its eco-friendly nature, abundant resources, low cost, non-toxic nature, significant absorption coefficient, and good conversion efficiency. Over the years, several studies on $BaSi_2$-based thin-film solar cells have been reported.[11,15–23] $BaSi_2$ is quite promising as an absorber material in thin film solar cells due to its high optical absorption coefficient, considerable minority-carrier diffusion length, long minority-carrier lifetime, good photoresponse spectra, and reasonably large surface recombination velocity. Recently, the study of $BaSi_2$ epitaxial films grown on tunnel junctions for thin-film solar cells and their photoresponsivity under various bias voltages was reported.[11] In general, the primary objective of any solar cell is to convert light energy into valuable electrical energy. The power conversion efficiency is a crucial parameter that can be used to identify a good solar cell material. The high efficiency of solar cells is indeed highly desirable and, in fact, essential to solving global power solutions. The efficiency can be assessed from the following dimensionless parameter:

$$\eta = \frac{J_{sc}\, V_{oc}\, FF}{P_s}, \tag{1}$$

$$FF = \frac{J_{\max}\, V_{\max}}{J_{sc}\, V_{oc}}, \tag{2}$$

where V_{oc} is the open circuit voltage, J_{sc} is short circuit current density, FF is the fill factor, η is the power conversion efficiency, and P_s is the power density of incident light. η of a solar cell material is directly related to V_{oc} and J_{sc}. All these solar cell parameters are influenced by the electronic structural properties of the solar cell material. The electronic bandgap of $BaSi_2$ is indirect with a magnitude of ∼1.3 eV and lies in the solar spectrum. Therefore, high η may be expected for $BaSi_2$. The $BaSi_2$ bandgap is close to that of conventional solar cell materials such as silicon. However, its light absorption has been reported to be higher than that of silicon. Thus, the photovoltaic performance of the $BaSi_2$ homojunction solar cell may be expected to be similar to that of silicon. For instance, in the case of p-$BaSi_2$/n-Si heterojunction grown by molecular beam epitaxy, V_{oc}, J_{sc}, and η have been reported to be 0.46 V, 31.9 mA/cm^2, and 9%, respectively.[24] For a boron-doped p-$BaSi_2$/n-Si solar cell, the reported magnitude of η is 10% and is highest ever reported for semiconducting silicides.[25] Furthermore, numerical studies performed on $BaSi_2$-based junctions with various doping densities have predicted η upto ∼22.5%.[26] The η of ∼20%–25% obtained from various parameters such as optical absorption coefficient, minority-carrier diffusion lengths, and minority-carrier lifetime has been reported for p^+–n abrupt homojunction.[27] Similarly, η of ∼28% has been predicted for a $CH_3NH_3PbI_3$/$BaSi_2$ (<2 μm) ultra-thin double-junction.[23] The abovementioned results clearly suggest that power conversion efficiency (η) can be quite high for $BaSi_2$, rendering it a promising material for solar cell applications.

Despite their practical importance, theoretical studies of photovoltaic (PV) parameters of $BaSi_2$ junctions are scarce. In particular, no *ab initio* quantum mechanical study of PV parameters of $BaSi_2$ that incorporates details at the atomic level has been reported to the best of our knowledge. Generally, the PV parameters are obtained from experimental data using continuum models.[28] Additionally, the continuum models can also be used to predict the performance of new device geometries. However, the major drawback of these models is that the inclusion of important effects such as strain, surface/interface effects, confinement of electrons and phonons, etc., becomes extremely challenging. However, these effects can be described in a reasonable detail in studies that use realistic atomic models and are based on the density-functional theory (DFT).[29] In recent years, the nonequilibrium Green's function (NEGF)[30] formalism combined with DFT has been successfully used to study transport properties of solar cells.[31]

As mentioned earlier, the bandgap of $BaSi_2$ is indirect, and therefore, absorption of a photon below the fundamental direct gap energy can take place only through the absorption or emission of a phonon in order to conserve momentum. This results in electron–phonon coupling (EPC) that is expected to play a critical role in indirect semiconductor PV cells.[32] Furthermore, recent studies have suggested that EPC plays an important role in the high performance of PV cells based on direct-bandgap materials.[33,34] In general, the computed magnitudes of some of the PV parameters can be expected to be severely underestimated if the EPC is ignored and excluded. It may be noted that, though EPC is important, its *ab initio* treatment in PV studies can be very challenging due to the involvement of complex two-excitation processes and double sum over fine grids of k-points.

Recently, a new efficient method named as special-thermal-displacement (STD) has been introduced for including phonon-induced absorption processes.[32] In the STD method, the atoms are displaced away from their equilibrium positions in the supercell. The STD approach combined with DFT-NEGF formalism has been recently used to study the first-order photocurrent in a silicon p–n junction and electron transport in silicon systems with a large number of atoms.[31,35]

In this study, we perform a comprehensive investigation of the temperature-dependent solar cell parameters such as photocurrent density, short circuit current density (J_{sc}), open circuit voltage (V_{oc}), fill factor (FF), and efficiency (η) of $BaSi_2$ p–n homojunction using an STD approach in combination with density functional theory (DFT) and nonequilibrium Green's function theory (NEGF).[31,35] The temperature dependence of solar cell parameters arises due to phonon-assisted absorption over the indirect bandgap of $BaSi_2$ and is important since it influences the performance of the device. The first-principles studies of temperature-dependent solar cell properties of $BaSi_2$ have not been reported to the best of our knowledge. In addition, we have also studied the photovoltaic properties of p–n homojunctions and compared the results with those obtained for $BaSi_2$ p–n homojunctions. Like semiconducting silicide $BaSi_2$, the compound $BaGe_2$ is an important semiconducting germanide with several promising applications.[36,37] The electronic structure of $BaGe_2$ is quite similar to that of $BaSi_2$. However, the EPC in this compound is expected to be disparate as compared to that in $BaSi_2$ due to the difference in phonon frequencies and spectrum. As temperature increases, phonons in the solar cell material play an important role through the EPC, affecting its performance. The phonon-assisted tunneling across the $BaSi_2$ and $BaGe_2$ p–n homojunction is expected to improve the key solar cell parameters V_{oc}, J_{sc}, and η. In fact, our study strongly suggests that the *ab initio* estimates of PV parameters can be significantly underestimated if the EPC is ignored and not included in the calculations. Additionally, our work demonstrates that *ab initio* quantum mechanical computations of various properties of solar cell devices, though challenging, can be successfully carried out.

The rest of the article is organized as follows. The computational details are presented in Sec. II. The discussion on the electronic structure and optical properties of bulk $BaSi_2$ is presented in Secs. III A and III B, respectively. The discussion on local density of states, photocurrent density, and $J-V$ characteristics of $BaSi_2$ ($BaGe_2$) p–n homojunctions is presented in Secs. III C, IV, and V, respectively. Finally, the conclusions are given in Sec. VI.

II. COMPUTATIONAL DETAILS

The temperature-dependent solar cell parameters are computed using DFT[29] and NEGF[30] methods as implemented in Quantum Atomistix Toolkit software.[38] The photocurrent is calculated by including the light–matter interaction in the NEGF from the first-order Born approximation. The electron–phonon coupling (EPC) is included through special thermal displacements.[32,35] The

exchange-correlation (xc) functionals are approximated using GGA + 1/2[39] and local density approximation (LDA)[40] schemes. Usually, the bandgaps of materials computed using LDA and GGA functionals are generally underestimated by ∼50% compared to their experimental values. Therefore, to overcome the bandgap problem, we use GGA + 1/2 scheme that is known to yield reasonably accurate bandgap of materials. The GGA + 1/2 scheme is also computationally inexpensive as compared to other schemes such as hybrid functionals (HSEs), GW, etc.[41] The Kohn–Sham orbitals are expanded using a double zeta-polarized LCAO basis set. An energy cut-off of 105 Ha (125 Ha) is used to expand the Kohn–Sham orbitals. The atomic positions are relaxed until the forces on each atom are reduced to less than 0.01 eV/Å. Self-consistency in the calculations is achieved by allowing the total energy converge to 10^{-6} eV/cell. The electronic structure (transport) calculations are performed by sampling the Brillouin zone using $12 \times 14 \times 9$ ($20 \times 16 \times 1$) Monkhorst–Pack k-point meshes. The phonon calculations are performed using generalized self-consistent force field potentials developed by Pedone *et al.*[38,42] Electronic doping is included by adding a charge fixed at the position of every atom in the structure.[30] The solar cell parameters are computed under a photon flux of 1 s^{-1} A^{-2}, p-side, and n-side-doped density of 3.5×10^{18} cm^{-3}. The NEGF method, the photocurrent calculation using the first-order Born approximation, phonon calculations, and the STD approach for inclusion of EPC are briefly summarized in the supplementary material.

III. RESULTS AND DISCUSSIONS

A. Crystal, electronic structures, and phonon properties of $BaSi_2$

We first briefly discuss the electronic structure of $BaSi_2$ since it directly influences the solar cell properties of the p–n junction. The bulk $BaSi_2$ crystallizes in an orthorhombic structure with space group *Pnma* (No. 62) symmetry.[22] Figure 1 shows the unit cell of $BaSi_2$, which contains 16 Si atoms at three crystallographic sites and 8 Ba atoms at two crystallographic sites.[43] The strong bonds are formed between the Si atoms that results in the formation of separate isolated Si_4 tetrahedra with T_h symmetry. The interatomic distance between the Si atoms in the isolated Si_4 tetrahedra is ∼2.38 Å and Ba to Si distance is ∼3.53 Å. The Born effective charges are used to understand the bonding nature in the $BaSi_2$, and computed values are consistent with our previous study.[43] Figure 2 shows the directional dependence of Born effective charge calculated as[44]

$$Z = (l_1^4 Z_{11} + l_1^2 l_2^2 Z_{12} + l_1^2 l_3^2 Z_{13} + l_2^2 l_1^2 Z_{21} + l_2^4 Z_{22} + l_2^2 l_3^2 Z_{23} + l_3^2 l_2^2 Z_{32} + l_3^2 l_1^2 Z_{31} + l_3^4 Z_{33}), \quad (3)$$

where l is the direction cosines of the Born effective charge tensor (Z_{ij}). Figures 2(a) and 2(b) show the Z_{ij} of Ba and Si atoms, respectively. As evident from Fig. 2, the Ba (Si) atoms have a more effective positive charge (effective negative charge) as compared to their nominal static charge values (Ba is +2e and Si is −1e). The charge is transferred from Ba to Si, and strong covalent bonds are formed between the Si atoms in the Si_4 cluster. The computed total and partial density of states (DOS) of bulk $BaSi_2$ are shown in Fig. 3(b).

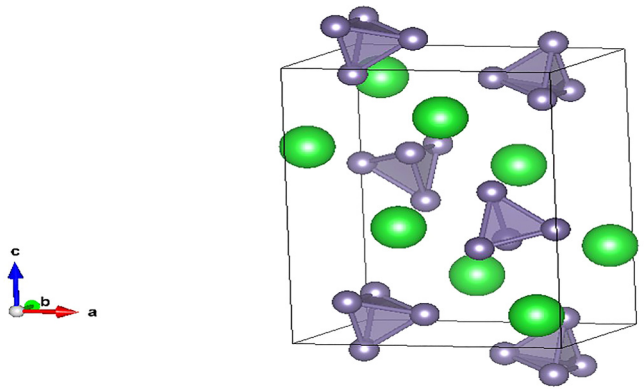

FIG. 1. The unit cell of orthorhombic $BaSi_2$ with Pnma symmetry. The Ba and Si atoms are indicated by green large balls and small gray balls, respectively.

In the VB, isolated Si_4 3p orbitals appear at significantly higher energy range of −0.5 to −4 eV. These orbitals play an important role in providing a large number of hole charge carriers in the p–n junction solar cells as further discussed in Secs. IV and V. The CB is primarily contributed by Ba-4d orbitals along with minor contribution from almost flat Ba-6s and Si-3p orbitals. Overall, the VB is mainly comprised of Si-3p orbitals, whereas CB is comprised of Ba-4d orbitals.

The computed band structure of $BaSi_2$ along a high symmetry direction is displayed in Fig. 3(a). As can be seen in Fig. 3(a), the VB maximum is found along the Γ–X path and CB minimum at L-point. The electronic bandgaps are computed for various exchange-correlation potentials and are listed in Table I. The indirect bandgaps (direct bandgap) of $BaSi_2$ computed using LDA and GGA are found to be 0.57 eV (0.62 eV) and 0.80 eV (0.87 eV), respectively. As expected, the LDA and GGA computed bandgaps are underestimated as compared to their experimental values. As discussed earlier, the GGA + 1/2 scheme has been successfully used, in recent years, to correctly estimate the bandgaps of several semiconductors.[39] The GGA + 1/2 method is a semi-empirical approach to correct the self-interaction error in semilocal exchange-correlation density functionals in the extended system. The band structure computed using the GGA + 1/2 scheme is shown in Fig. 3(a). The indirect (direct) bandgap of $BaSi_2$ computed using GGA + 1/2 is found to be 1.22 eV (1.39 eV), which is in good agreement with the experimental value of 1.25 eV. Overall, the results for the crystal structure, born effective charges, and the electronic structure are found to be in good agreement with previously reported theoretical and experimental values.[6,15,17,43,47]

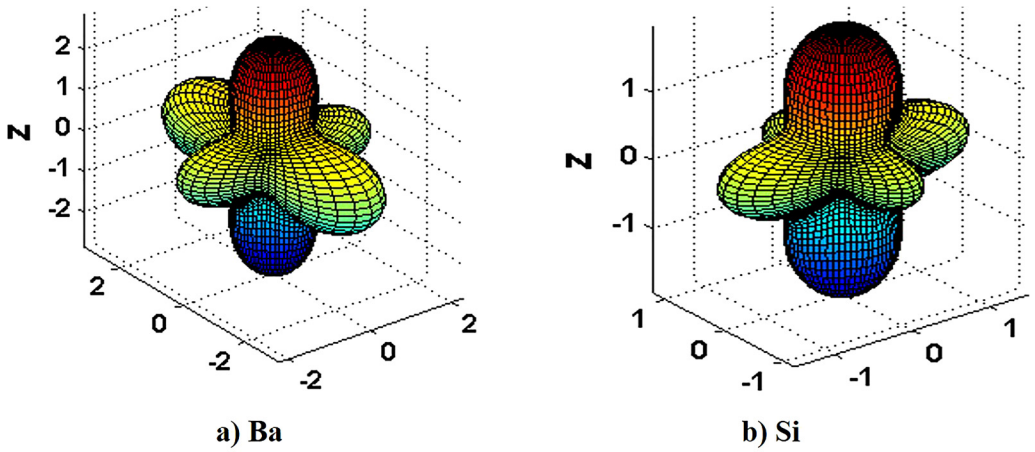

FIG. 2. Computed directional dependent Born effective charges in $BaSi_2$. (a) Born effective charges of the Ba atom; (b) Born effective charges of the Si atom.

We have also computed the phonon dispersions using generalized self-consistent force field potentials of Pedone *et al.*[38,42] Phonon dispersion along the high-symmetry path in the Brillouin zone and its phonon density of states for bulk $BaSi_2$ and $BaGe_2$ are displayed in Figs. 3(c) and 3(d). The results are consistent with those obtained using *ab initio* DFT and GGA functional as reported.[45] The phonon dispersion of both materials has almost similar features in different phonon energy ranges. The acoustic phonons of $BaSi_2$ ($BaGe_2$) are primarily obtained in the energy ranges of 0–11 meV (0–6 meV) due to heavy element Ba atomic vibrations. Similarly, optical phonons are quit flat and primarily obtained in the energy ranges of 10–59 meV (7–36 meV) due to the atomic vibrations of Si_4 (Ge_4). The acoustic and optical phonons are overlapped in the energy range of ∼4–7 meV (∼7–12 meV). As can be seen, the $BaSi_2$ phonon energies are much higher than those for $BaGe_2$ due to the significant mass difference between Si and Ge (Si atomic mass is 2.59 times that of Ge atom). This mass difference also results in broader phonon frequency range ($0 < h\nu < 60$ meV) in $BaSi_2$ as compared to that in $BaGe_2$ ($0 < h\nu < 37$ meV). The phonon dispersions also indicate that $BaSi_2$ and $BaGe_2$ are dynamically stable. These phonon results are relevant for understanding the temperature-dependent photocurrent discussed in Sec. IV and *J*–*V* characteristic in Sec. V.

B. Optical properties

The absorption of light energy is an essential parameter of the solar cell, and it can be assessed from the electronic structural properties of its constituent materials. A strong absorption coefficient of the absorber material is indeed desirable in solar cell applications. The absorption coefficient and optical bandgap are computed using the GGA + 1/2 scheme and within independent-particle approximation.[46] The absorption coefficient is anisotropic and its average value is calculated as $\alpha(\omega) = \{\alpha^{xx}(\omega) + \alpha^{xx}(\omega) + \alpha^{xx}(\omega)\}/3$. The average absorption coefficient of $BaSi_2$ as a function of photon energy is shown in Fig. 4(a). The absorption coefficient can be seen to increase from zero for energies more than the indirect bandgap due to electrons transfer from VB maximum [along Γ(000)—X(0.5 0 0) path] to CB minimum [L (0.5 0 0.5)] point. In particular, at the onset of absorption, the electrons are transferred from VB maximum (along Γ–X point) comprised of primarily Si-3*p* orbitals to CB minimum (at L point) comprised of primarily Ba-6*s*4*d* and Si-3*p* orbitals. These inter-band transitions are responsible for obtaining the absorption onset and optical bandgap (see Fig. 4). The optical bandgap of 1.41 eV is obtained from the extrapolation line shown in Fig. 4(b). The absorption onset is about 1.16 eV, close to the bandgap of $BaSi_2$, as reported in Table I. Figure 4(a) shows a significant absorption coefficient (>10^4 cm^{-1}) for low photon energy around ∼1.2 eV, which indicates that $BaSi_2$ should be a potential candidate for solar cell applications. As can be seen in Fig. 4(a), the absorption sharply increases in the light energy range of 1.6–3 eV due to semi-localized nature and thereby flat dispersion of states of Ba and Si atoms in the CB (0.7–2.5 eV). It may be noted that the absorption in $BaSi_2$ as a function of energy is different from that for conventional materials such as Si, GaAs, and Ge. The strong light absorption in the energy range of 3–8 eV is primarily obtained due to the transfer of electrons from Si-3*p* orbitals in the VB to Ba-4*d* orbitals in the CB. The above results are consistent with previously published ones since the GGA + 1/2 scheme provides reasonably accurate description of the band structure and density of states as discussed in Sec. III A.[15–17,47]

Next, we analyze the phonon-assisted absorption coefficient, which is important for understanding temperature-dependent solar cell properties. The phonons play a vital role in indirect bandgap semiconductors, such as $BaSi_2$, in promoting the electrons from VB to CB. The absorption coefficient (α) has square dependence on phonon energies as[48]

$$\alpha = (E - E_g \pm E_p)^2, \tag{4}$$

where E is photon energy, E_g is bandgap, and $+E_p$ ($-E_p$) is the phonon energy of absorption (emission). According to Eq. (4), the optical absorption in the material starts when the photon energy is

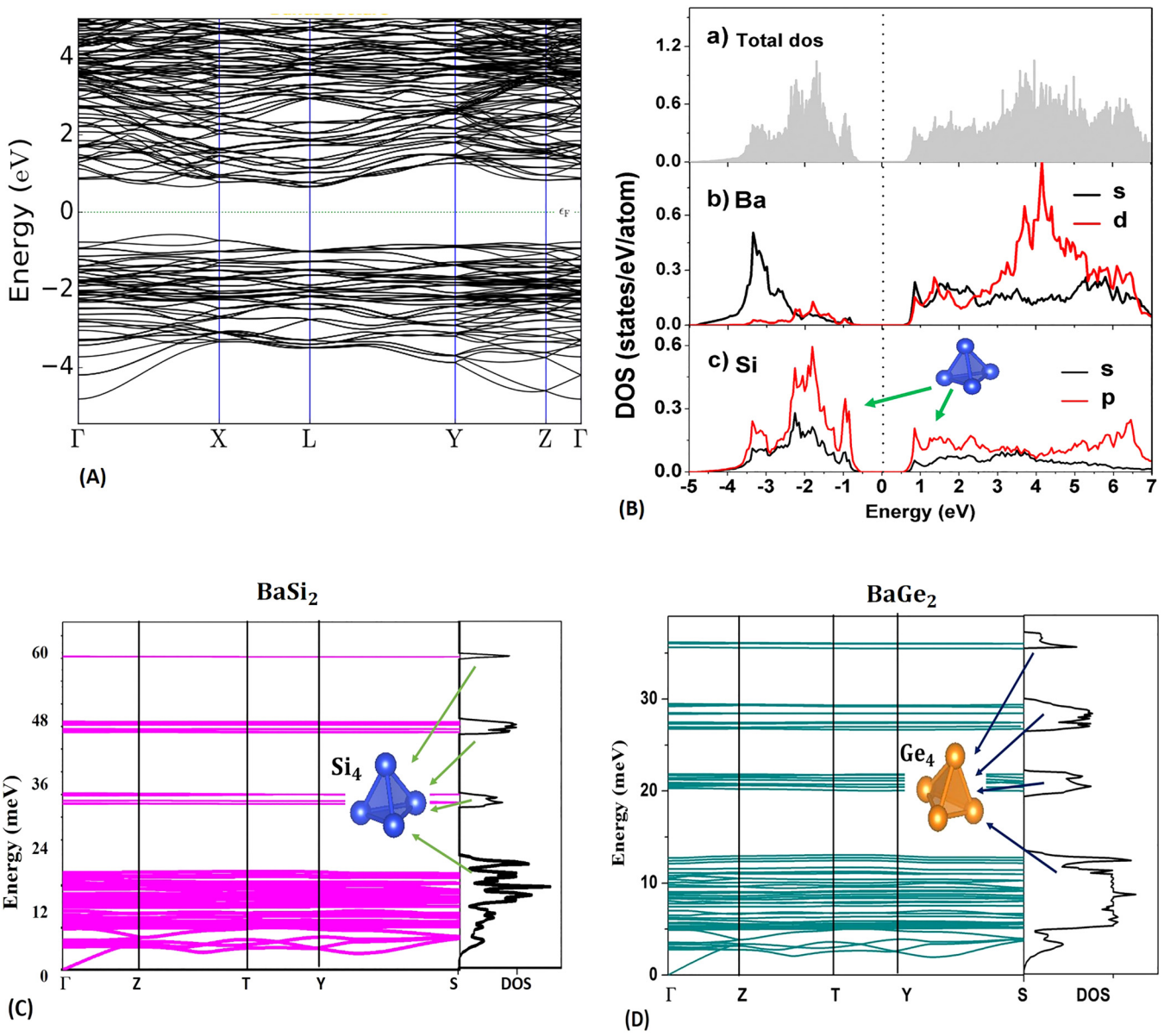

FIG. 3. Computed (GGA + 1/2) electronic properties of $BaSi_2$ (A) energy band structure along high symmetry directions. (B) Density of states: (a) total; (b) projected on the Ba atom; and (c) projected on the Si atom. (C) The phonon dispersion and phonon density of states for $BaSi_2$ and (D) $BaGe_2$ computed using generalized self-consistent force field potentials developed by Pedone *et al.*[38,42]

around the indirect bandgap of the semiconductors. In this case, phonon absorption or emission may influence the absorption coefficient even at 0 K. Therefore, the absorption coefficient can be varied evenly as compared to that for direct bandgap semiconductors like GaAs. As can be seen in Fig. 4(a), the absorption coefficient in the energy range of ∼1 to ∼1.4 eV evenly increases by the phonon effect. This phonon-dependent absorption coefficient is helpful in understanding the temperature-dependent solar cell properties. For instance, photocurrent properties are influenced by its phonon effect via the absorption coefficient, which is analyzed in Sec. IV.

C. Local density of states of $BaSi_2$ (100) *p–n* junction

Next, we analyze the crystal structure of the $BaSi_2$ (100) *p–n* junction and its electronic structural properties. The crystal

TABLE I. Lattice parameters and bandgaps of $BaSi_2$ and $BaGe_2$ computed using various XC functionals.

			a (Å)	b (Å)	c (Å)	E_g (eV)
$BaSi_2$	Cal.	LDA	8.84	6.67	11.42	0.57
		GGA	8.92	6.72	11.47	0.80
		GGA+1/2	8.95	6.78	11.48	1.22
	Exp.[a]		8.94	6.73	11.55	1.25
$BaGe_2$	Cal.	LDA	8.98	6.75	11.45	0.53
		GGA	9.05	6.81	11.57	0.76
		GGA+1/2	8.99	6.75	11.54	1.02
	Exp.[b]		9.07	6.82	11.65	1.0

[a]Ref. 8.
[b]Ref. 37.

structure of $BaSi_2$ (100) p–n homojunction is shown in Fig. 5(a), which is formed by repeating the unit cell nine times (total length is 80.5 Å) along with X-axis. The left and rights parts are doped as p-type and n-type, respectively, with a doping density magnitude of 5×10^{19} cm^{-3}, as shown in Fig. 5(a). The $BaGe_2$ (100) p–n junction is also modeled and constructed similarly. The local density of states (LDOS) for $BaSi_2$ (100) p–n junction is simulated using the DFT and NEGF method. The LDOS calculation methodology is briefly described in the supplementary material. The computed LDOS is shown in Fig. 5(b); the black and blueberry colors indicate the absence and presence of the electron density of states, respectively. The Fermi level is located at 0 eV. The left electrode ($\in_L$) side Fermi level is near to the valence band indicating p-type nature, whereas the right electrode ($\in_R$) side Fermi level is near to the conduction band indicating n-type nature. A p–n junction region is located around 40 Å, which shows a bit narrow bandgap as compared to that at electrodes. Therefore, the bandgap smoothly reduces from electrodes to the p–n junction. The bandgap (1.20 eV) at the electrode region matches with the bandgap of bulk $BaSi_2$ (see Table I).

IV. PHOTOCURRENT DENSITY OF $BaSi_2$ AND $BaGe_2$ p–n JUNCTIONS

The photocurrent density primarily depends on the electronic structural and optical properties. The $BaSi_2$ (100) p–n junction [see Fig. 5(a)] and $BaGe_2$ (100) p–n junction are used in the photocurrent calculation under standard AM1.5 illumination with a photon flux of 1 s^{-1} Å^{-2}. The EPC has been applied through the STD scheme to describe the effect of the temperature on the photocurrent. Figure 6 illustrates the GGA + 1/2 and LDA-computed photocurrent density of the $BaSi_2$ p–n junction. The electron–hole pairs are generated due to the excitation of VB electrons to CB as the $BaSi_2$ (100) atomic layers [see Fig. 5(a)] absorb the light energy. For photon energy less than 3 eV [see Fig. 6(a)], the hole charge carriers primarily come from 3p orbitals of the silicon cluster (Si_4) in the VB, whereas the electron charge carriers come from Ba-4d6s orbitals and Si-3p orbitals in the CB. For photon energy greater than 3 eV, the hole charge carriers primarily emerge from 3p orbitals of the silicon cluster (Si_4) in the VB, and the electron charge carriers emerge primarily from Ba-4d orbitals along with minor contribution from Ba-6s and Si-3p orbitals in the CB. In the case of $BaGe_2$, the hole charge carriers primarily emerge from 3p orbitals of the germanium cluster (Ge_4) in the VB, whereas electron charge carriers emerge from Ba-4d orbitals in the CB. The abovementioned charge carriers are responsible for photocurrent density, as shown in Fig. 6. A strong photocurrent is obtained (closed to the first order) due to significant optical absorption. It significantly increases in the energy range of 0.9–1.4 eV due to the indirect bandgap being close to the direct bandgap. Moreover, phonons assist interband transitions also play an important role at 300 and 400 K. The photocurrent depends on device potential and phonon assist tunneling at higher temperatures. In general, photocurrent starts with the photon energy becoming higher than the material bandgap. However, in the case of the GGA + 1/2 scheme at 300 K, the photocurrent density of $BaSi_2$ and $BaGe_2$ initializes at a photon energy of 0.88 and 0.75 eV, respectively. These values are lower by 0.34 eV for $BaSi_2$ and 0.24 eV for $BaGe_2$ as compared to their fundamental bandgaps. The bandgap is reduced with an increase in

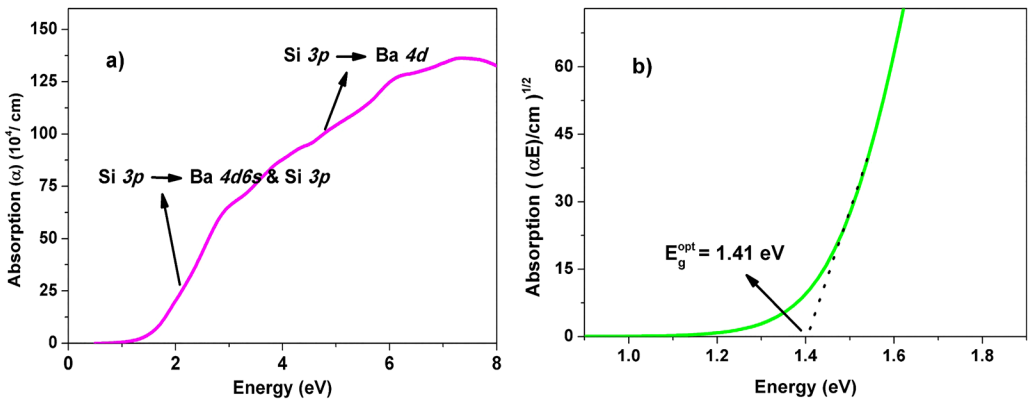

FIG. 4. The computed (GGA + 1/2) optical properties of $BaSi_2$. (a) Absorption coefficient (α) as a function of light energy; (b) optical bandgap.

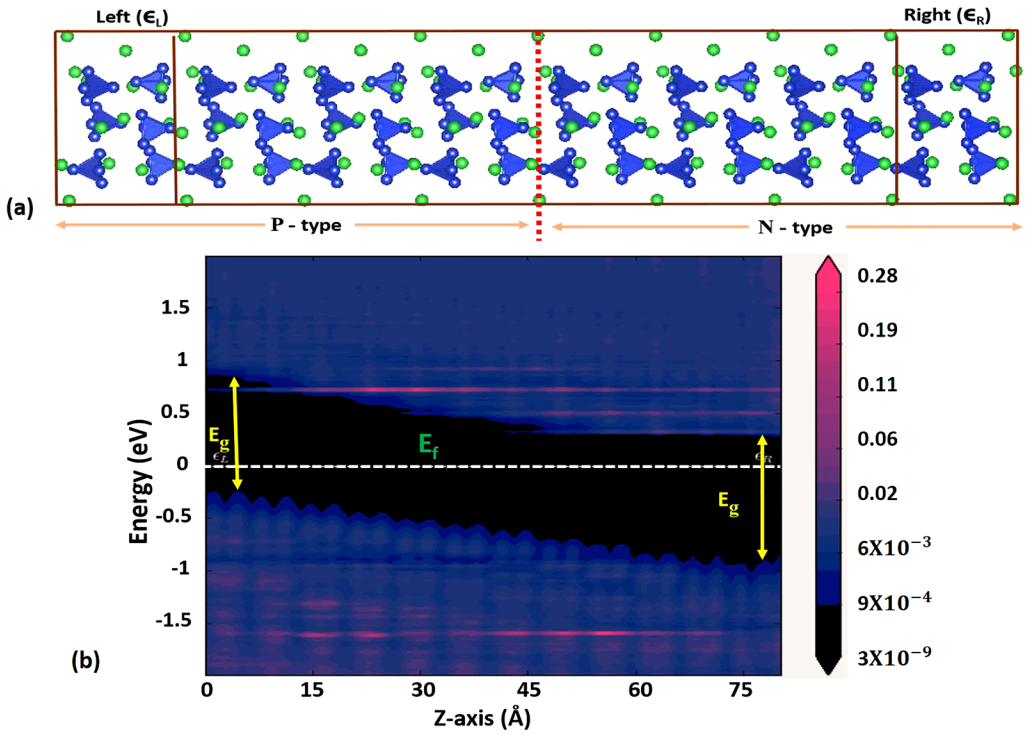

FIG. 5. (a) Crystal structure of $BaSi_2$ (100) p–n junction with doping density magnitude of 5×10^{19} cm^{-3}. Green and blue balls indicate Ba and Si atoms, respectively. (b) Local density of states (LDOS) for $BaSi_2$ (100) *p–n* junction at equilibrium and computed using the DFT + NEGF method.

temperature due to the phonon effect. Therefore, the optical absorption [Eq. (4)] and the photocurrent density are shifted toward the lower energy side.[35,48] In addition, the temperature-dependent photocurrent shift toward the lower energy side is also due to the charge carrier interaction with the phonons in the $BaSi_2$ and $BaGe_2$ *p–n* junction. The LDA results are almost similar to those obtained using GGA + 1/2. The LDA-computed photocurrent density starts near the indirect bandgap. At temperature 400 K, the photocurrent density computed using GGA + 1/2 (LDA) starts at 0.76 eV (1.05 eV) as shown in Figs. 6(a) and 6(b). As can be seen, the photocurrent density is shifted toward the lower energy side by ∼0.12 eV (0.17 eV) as compared to that at 300 K. Similarly, the

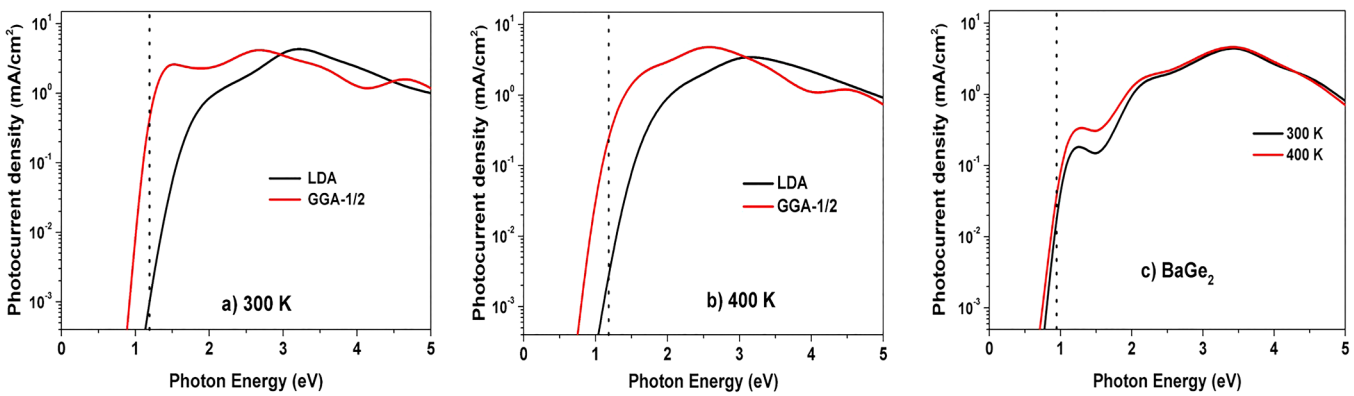

FIG. 6. GGA + 1/2 and LDA computed photocurrent density of STD configuration of $BaSi_2$ (100) *p–n* junction for temperatures (a) 300 and (b) 400 K. (c) GGA + 1/2 computed photocurrent density of $BaGe_2$ (100) *p–n* junction. The dotted line indicates the indirect bandgap position.

photocurrent density of $BaGe_2$ is shifted to lower energy by ~0.1 eV as compared to at 300 K. This shift increases with an increase in temperature due to the strong phonon population from external and internal vibrational modes of Ba, Si, and Ge atoms. These phonons interact with charge carriers.[43,45,49] As shown in Figs. 6(a) and 6(c), the photocurrent of $BaSi_2$ is stronger than that for $BaGe_2$ for light energy less than 1.5 eV. The strong photocurrent is due to the wide range of optical phonon density [33.12–60.30 meV, see Figs. 3(c) and 3(d)] of Si_4 tetrahedra compared to Ge_4.[43,45,49] This strong optical phonon density in the wider frequency range interacts with charge carriers across the *p–n* junction, which boosts the phonon assist tunneling of charge carriers across the *p–n* junction. Thus, the photocurrent of $BaSi_2$ is stronger than that of $BaGe_2$ due to EPC. Overall, the GGA + 1/2 results are expected to be more accurate compared to those obtained using LDA. The above results are also found to exhibit qualitatively trends similar to those reported for the silicon *p–n* junction study.[35]

V. *J* – *V* CHARACTERISTIC OF $BaSi_2$ and $BaGe_2$ *p–n* JUNCTIONS

In this section, we analyze the current density (J) as a function of the bias voltage (V) for temperatures 300 and 400 K. The crystalline $BaSi_2$ (100) *p–n* junction solar cell [see Fig. 5(a)] is used in the calculation under illumination condition. The computed least-square fit data points of current densities are used in the *p–n* junction diode equation,[35]

$$I = I_{ph} + I_0\left(\exp\left(\frac{qV}{nk_bT}\right) - 1\right), \tag{5}$$

where I_{ph} is the photocurrent, V is voltage, T is temperature, k_b is Boltzmann constant, and q is a charge. The $J - V$ characteristics fundamentally depend on the band structure and density of states of $BaSi_2$ as discussed in Sec. III A. In general, open circuit voltage V_{oc} is directly proportional to the electronic bandgap.[48] Therefore, the material with large bandgap may have large V_{oc} compared to that for low bandgap materials. The Fermi energy is located at the middle of the bandgap, and thus, the short circuit current density J_{sc} can be expected to arise due to electron and hole charge carriers. The large J_{sc} emerges primarily from the charge carriers of Ba-4*d* and Si_4-3*p* atomic orbitals and due to the minor contribution from Ba-6*s* and Si-3*s* orbitals (in Si_4 tetrahedra) (see Fig. 3). In $BaGe_2$, the hole charge carriers are primarily obtained from Ge-3*p* atomic orbitals. In the $BaSi_2$ ($BaGe_2$) crystal, the charge carriers contributed by Si(Ge) atoms are higher than those by Ba atoms since Si (Ge) atoms are twice as compared to Ba atoms. Therefore, as expected, the charge carriers contributed by Si_4 (Ge_4) atoms play an important role in the generation of high J_{sc}. The $J - V$ characteristics at $T = 300$ K and $T = 400$ K computed using GGA + 1/2 and LDA schemes are shown in Figs. 7(a) and 7(b), respectively. Figure 7(a) shows that dark current density (sunless) looks like that for a general *p–n* junction in the forward bias. For the GGA + 1/2 scheme at 300 K case, the J_{sc} is 27.35 mA/cm^2, V_{oc} is 0.84 V, and *FF* is 76.02%, with η of 18.01%. It may be noted that the EPC effect at various temperatures are taken into account in our calculations of these photovoltaic parameters. Our computed results at 300 K and 9 nm length of *p–n* junction with a doping density of 5×10^{19} cm^{-3} are in qualitative agreement with reported previous studies.[26,50] However, photovoltaic parameters are overestimated in these earlier studies as compared to results presented in this study due to neglect of EPC contributions. Figure S1 in the supplementary material shows the V_{oc} computed (GGA + 1/2) as function of the temperature in the range 100 K $\leq T \leq$ 400 K. As expected, the V_{oc} is found to decrease almost linearly with the temperature.

In the case of $BaGe_2$, J_{sc}, V_{oc}, *FF*, and η are found to be 26.12 mA/cm^2, 0.78 V, 80.02%, and 16.56%, respectively [see Fig. 7(c) and Table II]. As discussed earlier, the crystal structure and bonding nature are almost similar for both semiconductors $BaSi_2$ and $BaGe_2$. However, their photovoltaic properties exhibit a small difference due to disparity in their bandgap. At $T = 300$ K, the computed J_{sc} for $BaGe_2$ is nearly same as that for $BaSi_2$, whereas V_{oc} is lower than that for $BaSi_2$. The computed J_{sc}, V_{oc}, *FF*, and η for $BaSi_2$ at $T = 400$ K are found to be 29.51 mA/cm^2, 0.67 V, 74.24%, and 15.20%, respectively. The V_{oc} is reduced by 0.17 V, whereas J_{sc} is increased by 2.16 mA/cm^2 as the temperature is increased from 300 to 400 K. As a result, the η is suppressed by 2.81% with the temperature increasing from 300 to 400 K. In the case of $BaGe_2$ at 400 K, J_{sc}, V_{oc}, *FF*, and η are computed to be 28.05 mA/cm^2, 0.62 V, 81.15%, and 14.31%, respectively. J_{sc} depends on the temperature-dependent Fermi–Dirac distribution of charge carriers and electron–phonon interaction at the *p–n* junction. As temperature increases, the number of free charge carriers increases due to the temperature dependence of Fermi–Dirac distribution. These large number of free charge carriers interact with phonons in the *p–n* junction. As the temperature increases, the probability of charge carriers tunnelling across the ultra-thin *p–n* junction also increases due to the increase in the strength of phonon density in the EPC process. The influence of the EPC in the charge carrier tunnelling is much higher as compared to that of Fermi–Dirac distribution for high temperatures. Thus, J_{sc} at 400 K is expectedly higher than that at 300 K due to the strong EPC. The electron–phonon (EPC) interaction in the $BaSi_2$ solar cell involves acoustic phonons in the frequency range of 0–12.40 meV [see Fig. 3(c)] and is associated with Ba atomic vibrations.[43,44,49]Similarly, the optical phonons contributing to EPC are in the frequency range of 33.12–60.30 meV [see Fig. 3(c)] and are associated with the atomic vibrations in Si_4 tetrahedra. As a result, J_{sc} at 400 K in $BaSi_2$ is higher by 2.16 mA/cm^2 as compared to that at 300 K. In the case of $BaGe_2$ solar cell, the electron–phonon interaction involves acoustic phonons with frequencies less than 11.3 meV and are due to Ba–Ge atomic vibrations [see Fig. 3(d)]. Likewise, the optical phonons in the frequency range of 16.62–35.60 meV contribute to EPC and are associated with the Ge_4 tetrahedra vibrations.[43,45,49] In $BaGe_2$, the increase in J_{sc} at 400 K as compared to that at 300 K is ~2.16 mA/cm^2. It may be noted that the atomic mass of Ge is more than twice as compared to Si atomic mass. Therefore, the optical phonon density of Si_4 clusters is much broader by ~23.07 meV [37.22–60.30 meV, see Figs. 3(c) and 3(d)] for $BaSi_2$ *p–n* junction as compared to phonon density of Ge_4 clusters for $BaGe_2$ *p–n* junction. This wider range of strong optical phonon density improves the phonon assist charge carrier tunneling across the $BaSi_2$ *p–n* junction solar cell. Thus, J_{sc} of the $BaSi_2$ solar cell is found to be higher than that of the $BaGe_2$ solar cell. However, J_{sc} remains nearly constant for different temperatures, whereas V_{oc} is significantly reduced due to the strong optical phonon population from

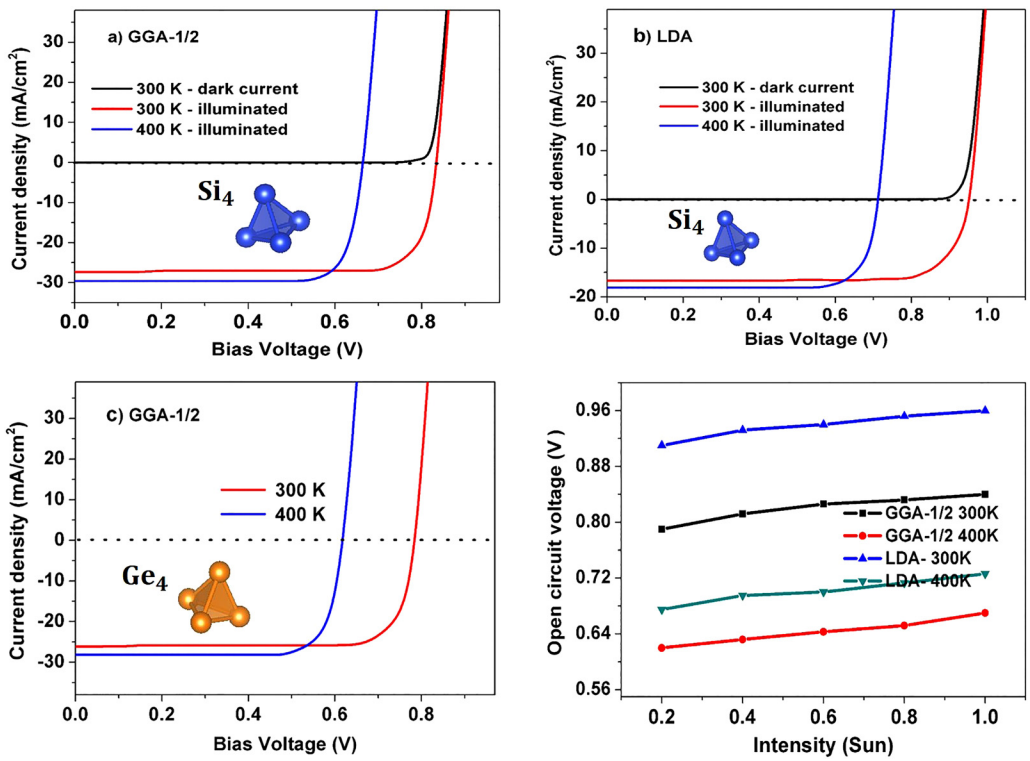

FIG. 7. *J–V* characteristics of STD atomic configuration of $BaSi_2$ (100) *p–n* junction at temperatures 300 and 400 K and computed using the DFT + NEGF method and (a) GGA + 1/2 scheme and (b) LDA scheme. (c) GGA + 1/2 results for $BaGe_2$ (100) *p–n* junction. (d) Open circuit voltage of $BaSi_2$ (100) *p–n* junction as a function of light intensity in the units of sun.

the internal and external vibrations of Si_4 (Ge_4) clusters. Therefore, temperature increases phonons of Si_4 (Ge_4) clusters, which results in the suppression of η. Both materials show suppression in η as the temperature is raised from 300 to 400 K (see Fig. 7). The crystal structure and the electronic structure of $BaSi_2$ and $BaGe_2$ are almost identical. However, their temperature-dependent photovoltaic properties exhibit disparity due to EPC effects, which, in turn, results from the difference in the Si and Ge masses. The LDA computed $J - V$ results are shown in Fig. 7(b) and listed in Table II. In the case of LDA at 300 K, we can observe that V_{oc} is high due to J_{sc} being substantially low as compared to that at GGA + 1/2 at 300 K. Thus, the LDA-computed solar efficiency is lower compared to that obtained using GGA + 1/2 at 300 K. At 400 K case, the LDA solar efficiency is further reduced due to reduction in V_{oc}. Overall, the solar efficiency computed using GGA + 1/2 is expected to be more accurate than that computed using LDA and those reported in previous studies.[26,50]

TABLE II. Computed photovoltaic properties of the $BaSi_2$ (100) *p–n* junction solar cell for 300 and 400 K. *T* is temperature, V_{oc} is open-circuit voltage, J_{sc} is short circuit current, *FF* is fill factor, and η is conversion efficiency.

	T (K)	J_{sc} (mA/cm^2)	V_{oc} (V)	*FF* (%)	η (%)
$BaSi_2$					
GGA+1/2	300	27.35	0.84	76.02	18.01
	400	29.51	0.67	74.24	15.20
LDA	300	16.75	0.95	70.6	11.20
	400	18.13	0.72	78.39	10.23
$BaGe_2$					
GGA+1/2	300	26.12	0.78	80.02	16.56
	400	28.05	0.62	81.15	14.31

The open-circuit voltage V_{oc} is an important parameter to analyze the solar cell properties. We have computed the V_{oc} of $BaSi_2$ (100) *p–n* junction using the GGA + 1/2 and LDA scheme for various light intensities, as demonstrated in Fig. 7(d). For the GGA + 1/2 (LDA) scheme at 300 K, the open-circuit voltage varies from 0.84 V (0.95 V) to 0.78 V (0.91 V) in the light intensity range of 0.2–1 sun. For 400 K, the magnitude of V_{oc} varies in the range of 0.67 V (0.72 V) to 0.62 V (0.67 V). These results indicate that V_{oc} increases by a small value with an increase in light intensity, which agrees qualitatively with results reported for Si *p–n* junction.[36]

VI. CONCLUSIONS

First principles investigations of temperature-dependent solar cell properties of $BaSi_2$ ($BaGe_2$) *p–n* homojunctions are performed using the density functional theory and the non-equilibrium

Green's function method. The special-thermal-displacement (STD) approach is used to introduce the electron–phonon coupling (EPC), which, in turn, is found to crucially affect the photocurrent and other solar cell parameters. The present study highlights the importance of phonon-assisted photon absorption and EPC in the computations of parameters such as photocurrent, open-circuit voltage (V_{oc}), short-circuit current (J_{sc}), and maximum power. As temperature increases, the photocurrent density is found to shift toward the lower photon energy side due to EPC. For temperature increasing from 300 to 400 K, J_{sc} is found to increase, whereas V_{oc} is found to decrease. The phonon-assisted tunneling in the $BaSi_2$ is found to be higher than that in $BaGe_2$ due to availability of phonons in the relatively wider frequency range arising from smaller mass of Si as compared to the mass of Ge atoms. The obtained quantitative results for $BaSi_2$ ($BaGe_2$) *p–n* homojunctions are expected to be useful and can be used as benchmark *ab initio* results in continuum model simulations. We hope that the present work will stimulate further *ab initio* quantum mechanical studies of solar cell devices and will be helpful in the experimental design of advanced solar cells with high photocurrent at low light energy.

SUPPLEMENTARY MATERIAL

See the supplementary material for complete details on various methodologies and other important results on photovoltaic properties of $BaSi_2$ and $BaGe_2$ *p–n* homojunction solar cell devices.

ACKNOWLEDGMENTS

The authors gratefully acknowledge the support from computational facilities provided by DST-FIST(SR/FST/PSI-215/2016).

AUTHOR DECLARATIONS

Conflict of Interest

The authors have no conflicts to disclose.

DATA AVAILABILITY

The data that support the findings of this study are available within the article.

REFERENCES

[1]V. E. Borisenko, *Semiconducting Silicides* (Springer, Berlin, 2000), Vol. 39, p. 348.
[2]D. M. Rowe, *CRC Handbook of Thermoelectrics* (CRC Press, Boca Raton, FL, 1994).
[3]D. Leong, M. Harry, K. J. Reeson, and K. P. Homewood, "A silicon/iron-disilicide light-emitting diode operating at a wavelength of 1.5 μm," Nature **387**, 686–688 (1997).
[4]M. Shaban, K. Nomoto, S. Izumi, and T. Yoshitake, "Characterization of near-infrared n-type β-$FeSi_2$/p-type Si heterojunction photodiodes at room temperature," Appl. Phys. Lett. **94**, 222113 (2009).
[5]J. Derrien, J. Chevrier, V. Lethanh, and J. E. Mahan, "Semiconducting silicide-silicon heterostructures: Growth, properties and applications," Appl. Surf. Sci. **56–58**, 382–393 (1992).
[6]D. Tsukahara, S. Yachi, H. Takeuchi, R. Takabe, W. Du, M. Baba, Y. Li, K. Toko, N. Usami, and T. Suemasu, "p-$BaSi_2$/n-Si heterojunction solar cells with conversion efficiency reaching 9.0%," Appl. Phys. Lett. **108**, 152101 (2016).
[7]W. Du *et al.*, "Analysis of the electrical properties of Cr/n-$BaSi_2$ Schottky junction and n-$BaSi_2$/p-Si heterojunction diodes for solar cell applications," J. Appl. Phys. **115**, 223701 (2014).
[8]T. Suemasu and N. Usami, "Exploring the potential of semiconducting $BaSi_2$ for thin-film solar cell applications," J. Phys. D: Appl. Phys. **50**, 023001 (2017).
[9]K. Hashimoto, K. Kurosaki, Y. Imamura, H. Muta, and S. Yamanaka, "Thermoelectric properties of $BaSi_2$, $SrSi_2$, and LaSi," J. Appl. Phys. **102**, 063703 (2007).
[10]R. A. McKee *et al.*, "$BaSi_2$ and thin film alkaline earth silicides on silicon," Appl. Phys. Lett. **63**, 2818 (1993).
[11]W. Du *et al.*, "Improved photoresponsivity of semiconducting $BaSi_2$ epitaxial films grown on a tunnel junction for thin-film solar cells," Appl. Phys. Lett. **100**, 152114 (2012).
[12]S. Yachi *et al.*, "Effect of amorphous Si capping layer on the hole transport properties of $BaSi_2$ and improved conversion efficiency approaching 10% in p-$BaSi_2$/n-Si solar cells," Appl. Phys. Lett. **109**, 072103 (2016).
[13]K. O. Hara *et al.*, "Realization of single-phase $BaSi_2$ films by vacuum evaporation with suitable optical properties and carrier lifetime for solar cell applications," Jpn. J. Appl. Phys. **54**, 07JE02 (2015).
[14]R. Takabe *et al.*, "Influence of grain size and surface condition on minority-carrier lifetime in undoped n-$BaSi_2$ on Si(111)," J. Appl. Phys. **115**, 193510 (2014).
[15]M. Kumar, N. Umezawa, and M. Imai, "$(Sr,Ba)(Si,Ge)_2$ for thin-film solar cell applications: First-principles study," J. Appl. Phys. **115**, 203718 (2014).
[16]K. Morita, Y. Inomata, and T. Suemasu, "Optical and electrical properties of semiconducting $BaSi_2$ thin films on Si substrates grown by molecular beam epitaxy," Thin Solid Films **508**, 363–366 (2006).
[17]T. Nakamura, T. Suemasu, K. Takakura, and F. Hasegawa, "Investigation of the energy band structure of orthorhombic $BaSi_2$ by optical and electrical measurements and theoretical calculations," Appl. Phys. Lett. **81**, 1032 (2002).
[18]M. Baba, M. Kohyama, and T. Suemasu, "First-principles study of twin grain boundaries in epitaxial $BaSi_2$ on Si(111)," J. Appl. Phys. **120**, 085311 (2016).
[19]M. Baba, S. Tsurekawa, K. Watanabe, W. Du, K. Toko, K. O. Hara, N. Usami, T. Sekiguchi, and T. Suemasu, "Evaluation of potential variations around grain boundaries in $BaSi_2$ epitaxial films by kelvin probe force microscopy," Appl. Phys. Lett. **103**, 142113 (2013).
[20]K. O. Hara, N. Usami, K. Nakamura, R. Takabe, M. Baba, K. Toko, and T. Suemasu, "Determination of bulk minority-carrier lifetime in $BaSi_2$ earth-abundant absorber films by utilizing a drastic enhancement of carrier lifetime by post-growth annealing," Appl. Phys. Express **6**, 112302 (2013).
[21]M. Baba, K. Watanabe, K. O. Hara, K. Toko, T. Sekiguchi, N. Usami, and T. Suemasu, "Evaluation of minority carrier diffusion length of undoped n-$BaSi_2$ epitaxial thin films on Si(001) substrates by electron-beam-induced-current technique," Jpn. J. Appl. Phys. **53**, 078004 (2014).
[22]M. Kumar, N. Umezawa, W. Zhou, and M. Imai, "Barium disilicide as a promising thin-film photovoltaic absorber: Structural, electronic, and defect properties," J. Mater. Chem. A **5**, 25293–25302 (2017).
[23]M. Ajmal Khan, K. O. Hara, W. Du, M. Baba, K. Nakamura, M. Suzuno, K. Toko, N. Usami, and T. Suemasu, "*In-situ* heavily *p*-type doping of over 10^{20} cm^{-3} in semiconducting $BaSi_2$ thin films for solar cells applications," Appl. Phys. Lett. **102**, 112107 (2013).
[24]C. T. Trinh, Y. Nakagawa, K. O. Hara, R. Takabe, T. Suemasu, and N. Usami, "Photoresponse properties of $BaSi_2$ film grown on Si (100) by vacuum evaporation," Mater. Res. Express **3**, 076204 (2016).
[25]S. Yachi, R. Takabe, H. Takeuchi, K. Toko, and T. Suemasu, "Effect of amorphous Si capping layer on the hole transport properties of $BaSi_2$ and improved conversion efficiency approaching 10% in p-$BaSi_2$/n-Si solar cells," Appl. Phys. Lett. **109**, 072103 (2016).
[26]Q. Deng *et al.*, "Numerical simulation and optimization of Si/$BaSi_2$ heterojunction and $BaSi_2$ homojunction solar cells," J. Phys. D: Appl. Phys. **52**, 075501 (2019).
[27]R. Vismara, O. Isabella, and M. Zeman, "Organometallic halide perovskite/barium di-silicide thin-film double-junction solar cells," in *Photonics for Solar Energy Systems VI* (SPIE, 2016), Vol. 98980J.

[28]M. Burgelman, P. Nollet, and S. Degrave, "Modelling polycrystalline semiconductor solar cells," Thin Solid Films **361–362**, 527 (2000).
[29]W. Kohn and L. J. Sham, "Self-consistent equations including exchange and correlation effects," Phys. Rev. **140**, A1133 (1965).
[30]M. Brandbyge, J. L. Mozos, P. Ordejon, J. Taylor, and K. Stokbro, "Density-functional method for nonequilibrium electron transport," Phys. Rev. B **65**, 165401 (2002).
[31]T. Gunst, T. Markussen, M. L. N. Palsgaard, K. Stokbro, and M. Brandbyge, "First-principles electron transport with phonon coupling: Large scale at low cost," Phys. Rev. B **96**, 161404 (2017).
[32]M. Zacharias and F. Giustino, "One-shot calculation of temperature-dependent optical spectra and phonon-induced band-gap renormalization," Phys. Rev. B **94**, 075125 (2016).
[33]J. Yang, X. Wen, H. Xia, R. Sheng, Q. Ma, J. Kim, P. Tapping, T. Harada, T. W. Kee, F. Huang, Y.-B. Cheng, M. Green, A. Ho-Baillie, S. Huang, S. Shrestha, R. Patterson, and G. Conibeer, "Acoustic-optical phonon up-conversion and hot- phonon bottleneck in lead-halide perovskites," Nat. Commun. **8**, 14120 (2017).
[34]H. Kim, J. Hunger, E. Cánovas, M. Karakus, Z. Mics, M. Grechko, D. Turchinovich, S. H. Parekh, and M. Bonn, "Direct observation of mode-specific phonon-band gap coupling in methyl ammonium lead halide perovskites," Nat. Commun. **8**, 687 (2017).
[35]M. Palsgaard *et al.*, "Efficient first-principles calculation of phonon-assisted photocurrent in large-scale solar-cell devices," Phys. Rev. Appl. **10**, 014026 (2018).
[36]J. T. Vaughey, G. J. Miller, S. Gravelle, E. A. Leon-Escamilla, and J. D. Corbett, "Synthesis, structure, and properties of $BaGe_2$: A study of tetrahedral cluster packing and other three-connected nets in zintl phases," J. Solid State Chem. **133**, 501–507 (1997).
[37]M. Imai, "Energy gap of alkaline-earth-metal digermanides $SrGe_2$ and $BaGe_2$," Phys. Status Solidi C **10**, 1728 (2013).
[38]S. Smidstrup *et al.*,"QuantumATK: An integrated platform of electronic and atomic-scale modelling tools," J. Phys.: Condens. Matter **32**, 015901 (2020).
[39]L. G. Ferreira, M. Marques, and L. K. Teles, "Approximation to density functional theory for the calculation of band gaps of semiconductors," Phys. Rev. B **78**, 125116 (2008).
[40]D. M. Ceperley and B. J. Alder, "Ground state of the electron gas by a stochastic method," Phys. Rev. Lett. **45**, 566 (1980).
[41]R. M. Martin, *Electronic Structure Basic Theory and Practical Methods* (Cambridge University Press, 2004).
[42]A. Pedone, G. Malavasi, M. C. Menziani, A. N. Cormack, and U. Segre, "A new self-consistent empirical interatomic potential model for oxides, silicates and silica-based glasses," J. Phys. Chem. B **110**, 11780–11795 (2006).
[43]M. Ramesh and M. K. Niranjan, "Phonon modes, dielectric properties, infrared reflectivity, and Raman intensity spectra of semiconducting silicide $BaSi_2$: First principles study," J. Phys. Chem. Solids **121**, 219–227 (2018).
[44]K. G. Prasad *et al.*, "Investigation of Raman modes and born-effective charges in $AgNb_{1/2}Ta_{1/2}O_3$: A density-functional and Raman scattering study," J. Am. Ceram. Soc. **99**(1), 332–339 (2016).
[45]H. Peng, C. L. Wang, J. C. Li, R. Z. Zhang, M. X. Wang, H. C. Wang, Y. Sun, and M. Sheng, "Lattice dynamic properties of $BaSi_2$ and $BaGe_2$ from first principle calculations," Phys. Lett. A **374**, 3797–3800 (2010).
[46]J. E. Sipe and E. Ghahramani, "Nonlinear optical response of semiconductors in the independent-particle approximation," Phys. Rev. B **48**, 11705 (1993).
[47]M. Kumar, N. Umezawa, and M. Imai, Appl. Phys. Express **7**, 071203 (2014).
[48]J. Nelson, *The Physics of Solar Cells* (Imperial College Press, 2003).
[49]Y. Terai *et al.*, "Polarized Raman spectra of $BaSi_2$ epitaxial film grown by molecular beam epitaxy," Jpn. J. Appl. Phys. **56**, 05DD02 (2017).
[50]H. Liao, Q. Deng, Y. Shen, G. Wang, S. Wang, and Y. Mao, "Theoretical analysis of doping concentration, layer thickness and barrier height effects on $BaSi_2$ based homojunction solar cells toward high efficiency," Solar Energy **201**, 857–865 (2020).